ISSN 1674-1056
http://cpb.iphy.ac.cn
http://iopscience.iop.org/cpb
中国物理 B
Chinese Physics
中国物理
Chinese Physics B

Distinctive distribution of defects in CdZnTe: In ingots and their effects on the photoelectric properties

Xu Fu(符旭), Fang-Bao Wang(王方宝), Xi-Ran Zuo(左希然), Ze-Jian Wang(王泽剑), Qian-Ru Wang(王倩茹), Ke-Qin Wang(王柯钦), Ling-Yan Xu(徐凌燕), Ya-Dong Xu(徐亚东), Rong-Rong Guo(郭榕榕), Hui Yu(于晖), Wan-Qi Jie(介万奇)
Citation: Chin. Phys. B . 2018, 27(3): 037302. **doi:** 10.1088/1674-1056/27/3/037302

Journal homepage: http://cpb.iphy.ac.cn; http://iopscience.iop.org/cpb

What follows is a list of articles you may be interested in

Topological hierarchy matters–topological matters with superlattices of defects

Jing He(何敬), Su-Peng Kou(寇谡鹏)
Chin. Phys. B . 2016, 25(11): 117310. **doi:** 10.1088/1674-1056/25/11/117310

Electronic transport of bilayer graphene with asymmetry line defects

Xiao-Ming Zhao(赵小明), Ya-Jie Wu(吴亚杰), Chan Chen(陈婵), Ying Liang(梁颖), Su-Peng Kou(寇谡鹏)
Chin. Phys. B . 2016, 25(11): 117303. **doi:** 10.1088/1674-1056/25/11/117303

Study on electrical defects level in single layer two-dimensional Ta_2O_5

Dahai Li(李大海), Xiongfei Song(宋雄飞), Linfeng Hu(胡林峰), Ziyi Wang(王子仪), Rongjun Zhang(张荣君), Liangyao Chen(陈良尧), David Wei Zhang(张卫), Peng Zhou(周鹏)
Chin. Phys. B . 2016, 25(4): 047304. **doi:** 10.1088/1674-1056/25/4/047304

Electron states scattering off line edges on the surface of topological insulator

Shao Huai-Hua, Liu Yi-Man, Zhou Xiao-Ying, Zhou Guang-Hui
Chin. Phys. B . 2014, 23(10): 107304. **doi:** 10.1088/1674-1056/23/10/107304

Conductance of metallic nanoribbons with defects

Deng Shi-Xian,Liang Shi-Dong
Chin. Phys. B . 2012, 21(4): 047306. **doi:** 10.1088/1674-1056/21/4/047306

Distinctive distribution of defects in CdZnTe:In ingots and their effects on the photoelectric properties*

Xu Fu(符旭)[1], Fang-Bao Wang(王方宝)[1], Xi-Ran Zuo(左希然)[1], Ze-Jian Wang(王泽剑)[1], Qian-Ru Wang(王倩茹)[1], Ke-Qin Wang(王柯钦)[1], Ling-Yan Xu(徐凌燕)[1], Ya-Dong Xu(徐亚东)[1], Rong-Rong Guo(郭榕榕)[1,2], Hui Yu(于晖)[1], and Wan-Qi Jie(介万奇)[1,†]

[1] *State Key Laboratory of Solidification Processing, and Ministry of Industry and Information Technology (MIIT) Key Laboratory of Radiation Detection Materials and Devices, Northwestern Polytechnical University, Xi'an* 710072, *China*

[2] *School of Opto-electronic and Communication Engineering, Xiamen University of Technology, Xiamen* 361024, *China*

(Received 5 December 2017; revised manuscript received 28 December 2017; published online 13 February 2018)

Photoelectric properties of CdZnTe:In samples with distinctive defect distributions are investigated using various techniques. Samples cut from the head (T04) and tail (W02) regions of a crystal ingot show distinct differences in Te inclusion distribution. Obvious difference is not observed in Fourier transform infrared (FTIR) spectra, UV–Vis–NIR transmittance spectra, and *I–V* measurements. However, carrier mobility of the tip sample is higher than that of the tail according to the laser beam induced current (LBIC) measurements. Low temperature photoluminescence (PL) measurement presents sharp emission peaks of D^0X and A^0X, and relatively large peak of D^0X (or A^0X) / $D_{complex}$ for T04, indicating a better crystalline quality. Thermally stimulated current (TSC) spectrum shows higher density of shallow point defects, i.e., Cd vacancies, In^+_{Cd}, etc., in W02 sample, which could be responsible for the deterioration of electron mobility.

Keywords: defects, Te inclusions, semiconducting II–VI materials, CdZnTe

PACS: 73.50.Gr, 73.61.Ga, 72.20.Jv, 68.55.Ln **DOI:** 10.1088/1674-1056/27/3/037302

1. Introduction

With high atomic number, large band gap, and high electron mobility–lifetime product ($\mu\tau$), the compound semiconductor of cadmium zinc telluride (CdZnTe, CZT) has been widely used as room-temperature x-ray and γ-ray detectors and other electro-optical devices.[1–3] The quality of this material is still restricted by various factors, like the point defects, linear defects, bulk defects, and non-uniformity of elemental distribution.[4] The CZT intentionally doped with the elements of group III (Al, Ga, In) or group VII (Cl, Br) can be incorporated on Cd sites to compensate for Cd vacancies and achieve high resistivity.[5,6] The inevitable intrinsic defects of dislocations could be formed by the additional stress in the solidification process. Tellurium-rich precipitates due to retrograde solubility and Te inclusions trapped by the growth interface present still severe problems for the commonly used modified vertical Bridgman (MVB) method and travelling heater method (THM).[7,8] It has been proved that both donor and accepter levels can be introduced by the intrinsic or extrinsic point defects.[9,10] The low charge collection in ion-beam induced charge (IBIC) images demonstrates transient charge losses around Te inclusions and dislocations.[11,12] All these defects can significantly degrade the crystal properties and consequently deteriorate the performances of devices. Thus, the comprehensive study of these defects is quite important for the better understanding of the crystal properties and detector performance. However, defects including point defects and Te inclusions in crystal always interact with each other and then are difficult to distinguish each other.

In this study we investigate CdZnTe:In crystal according to the distinctive Te inclusion distribution along the growth direction, and correlate the distribution with the crystal growth process. The photoelectric properties of CZT crystals are investigated using the techniques of Fourier transform infrared (FTIR) transmission spectrum, UV–Vis–NIR transmittance spectrum, *I–V* and laser beam induced current (LBIC) measurements. Finally, the distribution of defect levels is studied and discussed by low-temperature photo-luminescence (PL) technique and thermally stimulated current (TSC) measurements to better illuminate the nature of the defect behaviors.

2. Experiment

Samples with dimensions of $5 \times 5 \times 2$ mm^3 were cut from the head (T04) and tail (W02) part of indium doped $Cd_{0.9}Zn_{0.1}Te$ crystal, grown by modified vertical Bridgman method in Imdetek Ltd Company. The surface damaged layers after slicing was removed by lapping, mechanical, and chemo-mechanical polish. The samples were then chemically etched

*Project supported by the National Natural Science Foundations of China (Grant Nos. 51502244, 51702271, U1631116, and 51372205), the National Key Research and Development Program of China (Grant Nos. 2016YFF0101301 and 2016YFE0115200), the Fund of the State Key Laboratory of Solidification Processing in Northwestern Polytechnical University, China (Grant No. SKLSP201741) the Natural Science Basic Research Plan in Shaanxi Province, China (Grant No. 2016KJXX-09), and the Fundamental Research Funds for the Central Universities, China (Grant No. 3102015BJ(II)ZS014).

†Corresponding author. E-mail: jwq@nwpu.edu.cn

© 2018 Chinese Physical Society and IOP Publishing Ltd

using 2% bromine methanol solution for 2 min, prior to the infrared transmittance microscopy, FTIR spectrometer and UV–Vis–NIR spectrometer measurements. For the laser beam induced current (LBIC) measurements, Au electrodes with the thickness of approximate 10–50 nm were fabricated on both surfaces of the samples and the excess carriers were produced by the pulsed laser with a wavelength of 527 nm, pulse width of 893 ps.

For the PL measurement, an argon ion laser with a wavelength of 488 nm was used as an excitation source. A Triax550 tri-grating monochromator and a photomultiplier tube (PMT) were employed to collect the luminescence emissions of the samples at 10 K with a spectral resolution of 0.3 nm. In the TSC measurement, the sample was cooled down to about 50 K in dark. Free carriers were excited by achromatic light from a halogen lamp with a wave length of 650 nm, and captured by defect traps at low temperature. As the temperature increased to 300 K in dark with a constant heating rate, the trapped carriers were thermally emitted and recorded under a volt bias of 10 V with the Keithley 6514 electrometer.

3. Results and discussion

Indium doped $Cd_{0.9}Zn_{0.1}Te$ ingot with a diameter of 60 mm and length of 180 mm is grown with the MVB method. The modified crystal growth parameters ensure the large grain size and less grain boundaries of CdZnTe: In crystals as shown in Fig. 1(a). Figures 1(b) and 1(c) show the IRTM images of samples T04 and W02, respectively. It can be seen that Te inclusions are uniformly distributed with an average concentration of $\sim 10^3$ cm^{-3} and size of $\sim$10 μm in W02 as shown in Fig. 1(c). However, Te inclusions in T04 are distributed in a belt-like zone with a bandwidth of $\sim$100 μm in the full range of sample thickness and no macroscopic Te inclusions are observed except those in the belt zone. It has been proved that Te-rich boundary layer formed in the melt of CdZnTe crystal could be

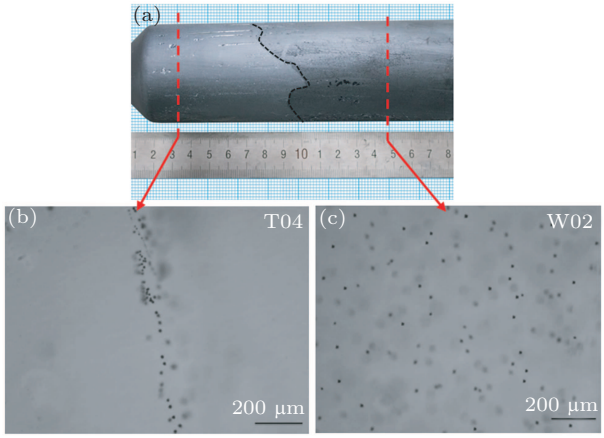


Fig. 1. (color online) Images of CdZnTe: In crystal grown with the MVB method, showing (a) image of asgrown CZT ingot, and ((b), (c)) IRTM images of T04 and W02 samples cut from the head and tail regions of the ingot, respectively.

captured by the growth interface and formed into Te inclusions.[13] Yang *et al.* concluded that grain boundaries could have a strong trapping effect of Te inclusions in the annealing process, which probably pass through the high-density zone of dislocation networks in the grain-boundary region.[14] Thus, we deduce that the Te inclusion belt could probably be formed through the trapping of Te atoms by sub-grain boundaries in the crystal growth process. This could also give an explanation of the "clean" zone near the Te inclusion belt (Fig. 1(b)).

Typical IR transmission spectra of the samples are shown in Fig. 2(a). The transmittance values of T04 and W02 reach 57.52% and 61.85%, respectively, and remain almost unchanged within the wave number of 1000–4000 cm^{-1}, which represents quite a good lattice perfection and crystalline quality of the ingot.[15] The same band gap values of the two samples (1.54 eV), as shown in Fig. 2(b), indicate that these two samples possess almost the same compositions. Moreover, good linear and symmetrical *I*–*V* results are observed even when subjected to a low bias voltage of ±0.1 V, as shown in Figs. 2(c) and 2(d). The bulk resistivity values are fitted to be 7.1×10^9 and 5.4×10^9 Ω·cm for T04 and W02, respectively. Combining the basic spectra and *I*–*V* measurements mentioned above, we can find that although the distribution and concentration of Te inclusions show distinctive difference, the general optical and electrical properties of these two samples are almost the same.

The LBIC waveforms measured with different bias voltages are shown in Figs. 3(a) and 3(c). The typical penetration depth of laser with a wavelength of 527 nm is around 530 nm in the CZT crystal, which is much less than the sample thickness. Thus, when negative bias is applied to the front electrode, the current signals are mainly induced by photogenerated electrons. The photocurrent response under 50 V bias voltage shows an instantaneous rising edge, with delay times of 3.8 ns and 4 ns reaching to the maximum values for T04 and W02, as shown in the inserts in Figs. 3(a) and 3(c), respectively. The linear relationships between the electron drift velocity and electric field strength are obtained in Figs. 3(b) and 3(d). Carrier drift velocity v can be calculated from the transit time t_R under a given bias voltage. The electron mobility is obtained from $v = \mu E$, where E is the applied electric field. The mobility of electron at room temperature in T04 is about 908 ± 18 cm^2/vs, which is higher than that in W02 (814 ± 16 cm^2/vs). It is considered that the carrier mobility is related to different scattering mechanisms. Xu *et al.*[16] concluded that for defect densities higher than 1×10^{17} cm^{-3} and lower than 1×10^{15} cm^{-3} in CZT, carrier mobility is limited by ionized impurity scattering and polar-optical phonon scattering, respectively. Thus, it is necessary to know the defect species and concentration in crystal for the better understanding of the carrier transport properties of the samples.

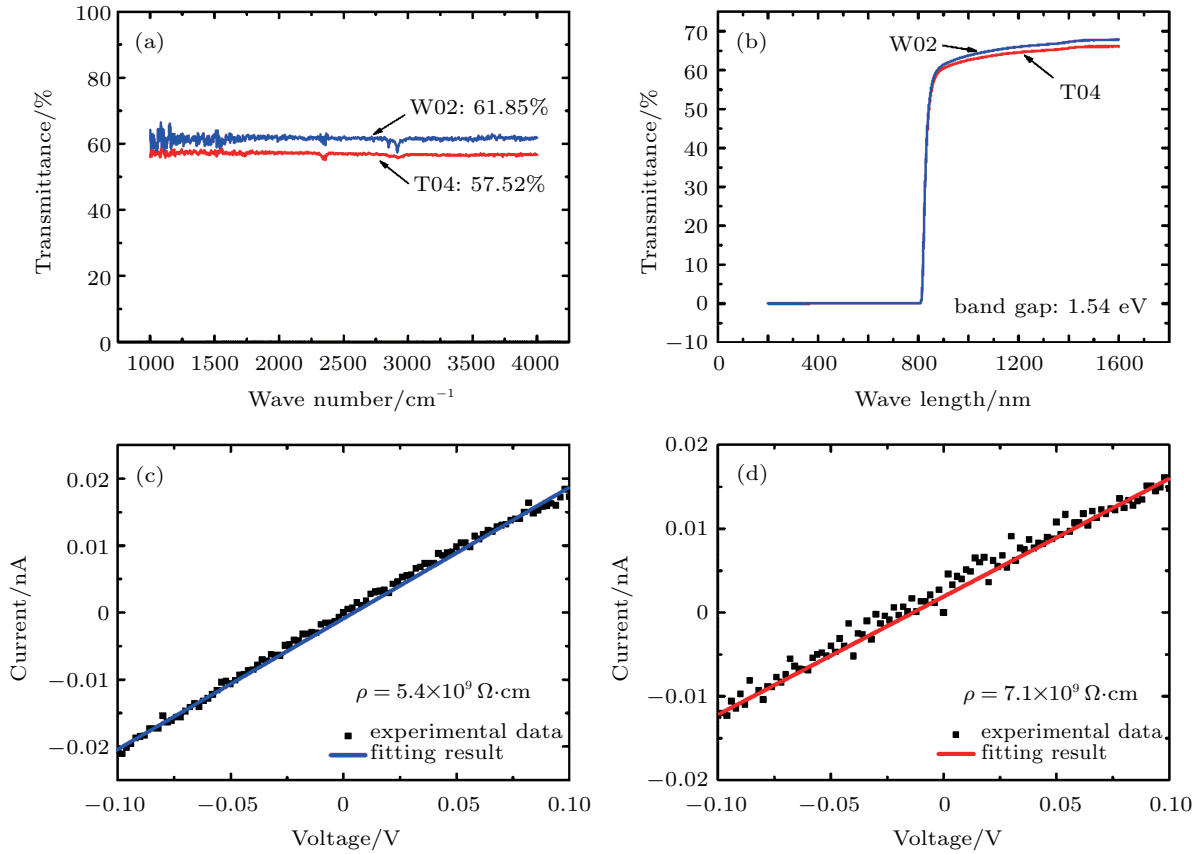


Fig. 2. (color online) (a) Typical FTIR transmission spectra, (b) UV–Vis–NIR transmittance spectra of T04 and W02 samples, ((c), (d)) *I*–*V* curves for W02 and T04, measured at room temperature, respectively.

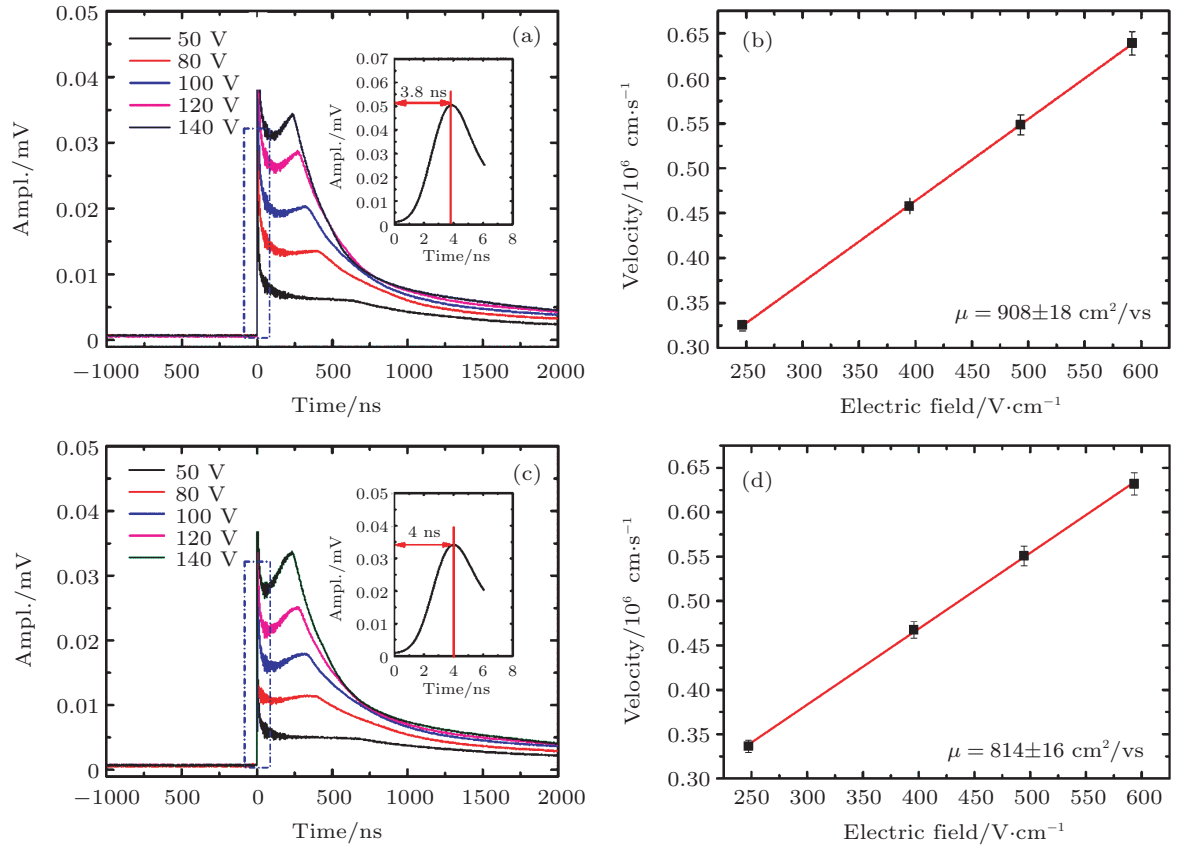


Fig. 3. (color online) LBIC measurements by exposing from cathode side, showing current waveforms for samples (a) T04 and (c) W02, and fitting results of electron mobility in the samples (b) T04 and (d) W02. Inserts in panels (a) and (c) are enlarged parts of the dotted blue rectangles.

As a sensitive technique for characterizing the types and distributions of defects and impurities in crystals, the low-temperature photo-luminescence spectrum is used to obtain the information about the recombination property of photo-carriers.[17–19] The FE peak is the recombination of the peaks of the free exciton, composite particles formed by the coulomb force of opposite charges. The emission peaks of D^0X and A^0X in PL spectrum originate from shallow donors (i.e., In_{Cd}, etc.)[20] and shallow acceptors (i.e., Li_{Cd}, Na_{Cd}, N_{Te}, etc.)[21,22] respectively. The DAP is emitted by the annihilation of shallow acceptors with shallow donors and the LO peaks are the longitudinal optical (LO) mode of direct electron-phonon interaction in CZT.[20]

Figure 4 shows the typical PL spectra of T04 and W02, ranging from 1.4 eV to 1.7 eV. For comparison, the measured data are normalized according to the emission peak intensity of $D_{complex}$. The sharp emission peaks of D^0X and A^0X, as well as the free exciton (FE) recombination are found for T04, indicating a better crystalline quality. In addition, the relative intensity of D^0X and DAP emission peaks in T04 is higher than that in A^0X, which shows the higher intensity of shallow donors in the T04 sample. For the asymmetry feature of $D_{complex}$, the peak is considered to consist of the structure defects and A-center in crystal.[12,23] It can be found that the intensity of $D_{complex}$ relative to other emission peaks from 1.58 eV to 1.65 eV shows that the relative intensity is much higher for W02 than that for T04, which also indicates that sample T04 has much better crystalline quality.

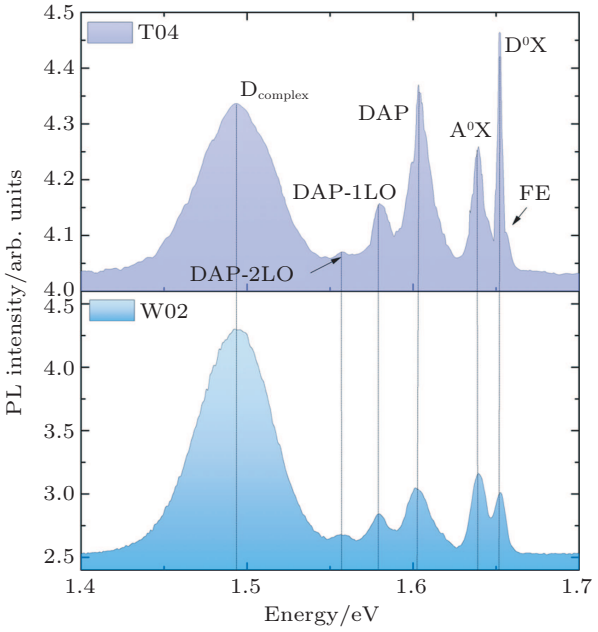


Fig. 4. (color online) Typical PL spectra of the samples T04 (upper) and W02 (lower).

Thermally stimulated current (TSC) measurements are used to investigate the deep-level defects in CZT crystals. Each peak in TSC spectrum corresponds to a certain trap level in the band-gap, and a certain defect state in the crystal lattice. In the experiment, the samples are illuminated for 10 min after the temperature has become stably lower than 50 K for 2 h, to make sure that all the defect levels are fully filled before temperature scanning. A heating rate of 0.2 K/s and bias voltage of 10 V are employed to record current spectra from 50 K to 300 K as shown in Fig. 5. A complete characterization of trap signatures in TSC spectra is simulated with the simultaneous multiple peak analysis (SIMPA) method proposed by Pavlovic *et al.*,[24] expressed as

$$I_{\mathrm{TSC}}(t) = N_{\mathrm{T}}\mu_n\tau_n eAED_t T^2 \exp\left\{-\frac{E_a}{kT} - \frac{kD_t T^4}{\beta E_a} \times \exp\left(-\frac{E_a}{kT}\right)\left[1 - 4\frac{kT}{E_a} + 20\left(\frac{kT}{E_a}\right)^2\right]\right\}, \quad (1)$$

where e is the electron charge, μ_n is the carrier mobility, τ_n is the carrier lifetime, A is the area of the electrode, E is the applied electric field, k is the Boltzmann constant, T is the absolute temperature, β is the heating rate, E_a is the thermal activation energy of the defects, N_T represents the carrier concentration of a given defect level at the beginning of the temperature ramp, and D_t is the temperature-dependent coefficient of the trap including capture cross section σ. The detailed parameter settings for CZT crystal can be seen in Ref. [25]. A total of seven trap peaks (T_1 to T_7) are identified from the TSC spectra of T04 and W02 (see Eq. (2)). Trap levels denoted as T1 and T2 are shallow defects appearing in the sample T04 only, with activation energies of 0.054 ± 0.01 eV and

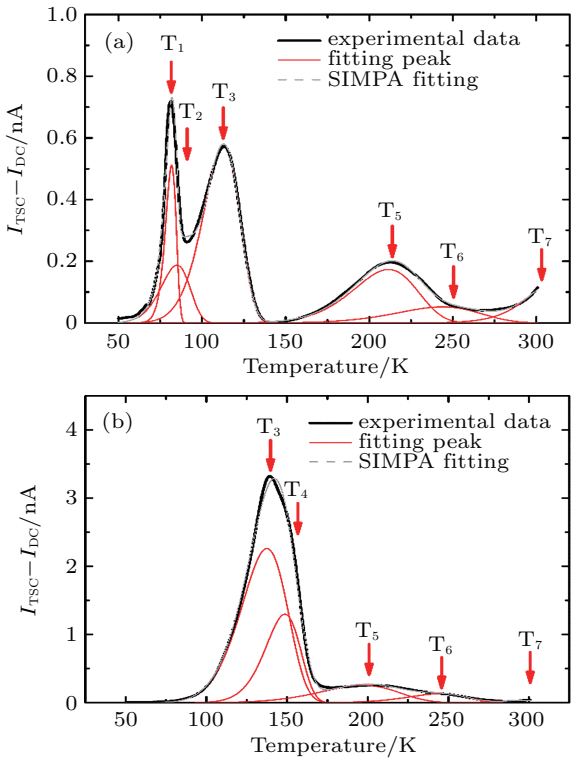


Fig. 5. (color online) Typical TSC spectra of amples (a) T04 and (b) W02.

0.056 ± 0.01 eV, which is considered as the A-center related defect levels.[26] The trap level T_3 (0.07 ± 0.01 eV) identified in both samples dominates the TSC current spectra and is assigned to a shallow donor originating at In dopant related point defect In_{Cd}^{+} by thermoelectric effect spectroscopy (TEES)[27] and by calculation.[28] Trap T_4 (0.08 ± 0.2 eV) appearing only in W02 due to the protuberance around 150 K is analyzed. For the sample cut from the tail part of the ingot, an enrichment of impurities can be formed. Thus, we speculate that this shallow defect level is associated with the impurities enriched during crystal growth. Traps T_5 and T_6 located at 0.14 ± 0.02 eV and 0.21 ± 0.02 eV above the valence band maximum respectively, are attributed to Cd vacancies or relevant defect complex.[28,29] Trap T_7 located at 0.56 ± 0.02 eV below the conduction band minimum can be attributed to the deep donor Te antisite (Te_{Cd}^{2+}) with the second ionization energy of ~0.59 eV according to theoretical calculations.[28]

A comparison of different trap densities between samples T04 and W02 is given in Table 1. We can see that the density of shallow defect levels of W02 before 150 K is one order higher than that of T04. Higher densities of T_5 and T_6 in Table 1 indicate higher Cd vacancies of W02. Correspondingly, higher densities of In_{Cd}^{+} (5.5×10^{15} cm^{-3} for T04 and 3.2×10^{16} cm^{-3} for W02) can be formed through In_{Cd}^{+}: In + $V_{Cd}^{-} \rightarrow In_{Cd}^{+}$ + 2e or In + $V_{Cd}^{2-} \rightarrow In_{Cd}^{+}$ + 3e.[30] Referring to IRTM images in Fig. 1, it can be concluded that the melt enrichment of Te solutions leads to not only Te inclusions, but also the shallow point defects like T_3 in the crystal growth process. These shallow defects with a total trap density of ~10^{17} cm^{-3} can probably dominate the scattering mechanism of these two samples as discussed above.

Table 1. Comparisons of the trap density in CdZnTe sample between samples T04 and W02.

	T_1	T_2	T_3	T_4	T_5	T_6	T_7
T04/cm^{-3}	1.6×10^{15}	1.5×10^{15}	5.5×10^{15}	-	1.2×10^{15}	2.8×10^{14}	1.4×10^{15}
W02/cm^{-3}	-	-	3.2×10^{16}	8.6×10^{15}	1.3×10^{15}	1.2×10^{15}	3×10^{14}

4. Conclusions

The optical and electrical properties of CdZnTe:In samples are intensively studied. The FTIR spectra and UV–Vis–NIR transmittance spectra show almost the same transmittance (57.52% and 61.85%) and the bandgap (1.54 eV), despite distinct difference in Te inclusion distribution between samples T04 and W02. Carriers' mobility values for T04 and W02 are measured with LBIC technique to be 908 ± 18 cm^2/vs and 814 ± 16 cm^2/vs, respectively. Sharp emission peaks of D^0X and A^0X, as well as the free exciton (FE) recombination in the PL spectrum indicate quite good crystalline quality of the T04 sample. Moreover, the intensity of $D_{complex}$ relative to other emission peaks between 1.58 eV to 1.65 eV is much higher for sample W02 than for samples T04. Seven trap peaks are identified from the TSC spectrum with the SIMPA method. The results show that higher densities of (5.5×10^{15} cm^{-3} for T04 and 3.2×10^{16} cm^{-3} for W02), Cd vacancies and relevant defect complex, could be formed in the crystal growth process, which probably dominates the scattering mechanisms of these two samples.

References

[1] Schlesinger T E, Toney J E, Yoon H, Lee E Y, Brunett B A, Franks L and James R B 2001 *Mater. Sci. Eng. R* **32** 103
[2] James R B, Brunett B, Heffelfinger J, Scyoc J V, Lund J, Doty F P, Lingren C L, Olsen R, Cross E and Hermon H 1998 *J. Electron. Mater.* **27** 788
[3] Eisen Y and Shor A 1998 *J. Cryst. Growth* **184** 1302
[4] Rudolph P 2010 *Defect Formation During Crystal Growth from the Melt* (Heidelberg: Springer Berlin Heidelberg) pp. 159–201
[5] Fiederle M, Fauler A, Konrath J and Babentsov V 2004 *IEEE T. Nucl. Sci.* **51** 1864
[6] Fiederle M, Eiche C, Salk M, Schwarz R, Benz K W, Stadler W, Hofmann D M and Meyer B K 1998 *J. Appl. Phys.* **84** 6689
[7] Rudolph P, Engel A, Schentke I and Grochocki A 1995 *J. Cryst. Growth* **147** 297
[8] Barz R U and Gille P 1995 *J. Cryst. Growth* **149** 196
[9] Castaldini A, Cavallini A, Fraboni B, Fernandez P and Piqueras J 1996 *J. Appl. Phys.* **83** 2121
[10] Zha G, Yang J, Xu L, Feng T, Wang N and Jie W 2014 *J. Appl. Phys.* **115** 103
[11] Gu Y, Rong C, Xu Y, Shen H, Zha G, Wang N, Lv H, Li X, Wei D and Jie W 2015 *Nucl. Instrum. Methods* **343** 89
[12] Fu X, Xu Y, Xu L, Gu Y, Jia N, Bai W, Zha G, Wang T and Jie W 2016 *Crystengcomm* **18** 5667
[13] Rudolph P, Neubert M and Uhlberg M M 1993 *J. Cryst. Growth* **128** 582
[14] Yang G, Bolotnikov A E, Fochuk P M, Camarda G S, Hossain A, Roy U N, Cui Y, Pinder R, Gray J and James R B 2014 *Phys. Status Solidi* **11** 1328
[15] Li G Q, Jie W Q, Gu Z and Hua H 2003 *Chin. Phys. Lett.* **20** 1600
[16] Xu L, Jie W, Fu X, Zha G, Feng T, Guo R, Wang T, Xu Y and Zaman Y 2014 *Nucl. Instrum. Methods* **767** 318
[17] Castaldini A, Cavallini A, Fraboni B, Fernandez P and Piqueras J 1996 *Appl. Phys. Lett.* **69** 3510
[18] Kim M D, Kang T W, Kim G H, Han M S, Cho H D, Kim J M, Jeoung Y T and Kim T W 1993 *J. Appl. Phys.* **73** 4074
[19] Seto S, Tanaka A, Masa Y and Dairaku S 1988 *Appl. Phys. Lett.* **53** 1524
[20] Jain S 2001 *Photoluminescence Study of Cadmium Zinc Telluride* (MS dissertation) (Morgantown: West Virginia University)
[21] Worschech L, Ossau W and Landwehr G 1995 *Phys. Rev. B* **81** 13965
[22] Halliday D P, Potter M D G, Mullins J T and Brinkman A W 2000 *J. Cryst. Growth* **220** 30
[23] Suzuki K, Inagaki K, Seto S, Tsubono I, Kimura N, Sawada T and Imai K 1996 *J. Cryst. Growth* **159** 388
[24] Pavlovic M, Desnica U V and Gladic J 2000 *J. Appl. Phys.* **88** 4563
[25] Pavlovic M, Jaksic M, Zorc H and Medunic Z 2008 *J. Appl. Phys.* **104** 8177
[26] Soundararajan R and Lynn K G 2012 *J. Appl. Phys.* **112** 431
[27] Lee E Y, James R B, Olsen R W and Hermon H 1999 *J. Electron. Mater.* **28** 766
[28] Wei S H and Zhang S B 2014 *Phys. Rev. B* **66** 155211
[29] Carvalho A, Tagantsev A K, Öberg S, Briddon P R and Setter N 2010 *Phys. Rev. B* **81** 075215
[30] Yu P, Jie W and Tao W 2011 *J. Mater. Sci.* **46** 3749